CFD Analysis of Impeller Design for A Respirator

Suresh Pittala
School of Mechanical & Industrial Engineering,
Hawassa University, P. O. Box – 5, Hawassa, Ethiopia.

Abstract

Designing impellers for respirator are important for fluid flow analysis. A new model is designed and analyzed for fluid flow using computational fluid dynamics (CFD). To improve the efficiency of pump, CFD analysis is used in the pump industry. In the present model Acrylonitrile butadiene styrene (ABS) material is used to reduce noise and cutting down the cost. The number of impeller blades is proposed to increase from 6-8 to 20 to increase fluid velocity. Inlet blade angle is reduced to less than 40 degrees from greater than 45 degrees to increase efficiency and outlet fluid velocity. From the CFD analysis, the velocity and pressure in the outlet of the impeller is outlet flow conditions are used to calculate the efficiency by using the empirical relations. In the first case outlet angle is increased, and in the second case inlet angle is decreased and they are obtained from the CFD analysis. It causes to improve efficiency.

KEY WORDS: Computational Fluid Dynamics (CFD) analysis, Impeller design, Respirator.

1. Introduction

The powered air purifying respirator (PAPR) specifically designed to protect health care professionals from residual chemical/ biological/ radiological agents when they are performing first responder duties during homeland security or terrorist situations. Weighing less than six pounds, the system features a lightweight, chemical-resistant belt-mounted blower with two HC CBA/ RCA canisters. The canisters contain a pleated high-efficiency (P-100) filter to remove aerosols, radio nuclides, and solid particulates, as well as an impregnated, activated carbon bed to adsorb (filter out) gases and vapors. Experimental setup of PAPR is shown

in fig.1.

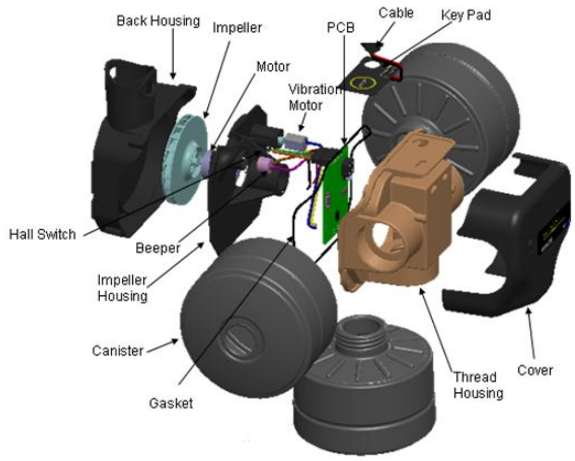

Fig.1. Experimental setup Powered Air Purifying Respirator (PAPR)

Impellers are prevalent for much different application in the industrial or other sector. Nevertheless, their design and performance prediction process is still a difficult task mainly due to the great number of free geometric parameters, the effect of which cannot be directly evaluated. The significant cost and time of the trial and error process by manufacturing and testing of physical prototype reduces the profit margins of the impeller manufacturers. For this reason CFD analysis is currently used in hydrodynamic design for different impeller types. Impeller is a rotating part of a centrifugal compressor/pump that imparts kinetic energy to a fluid. Here under we introduced (1) modeling laws and (2) Vibration and noise [1, 2].

1.1 **Modeling Laws** The modeling laws includes both the affinity law and model law. These two laws are stated below:

1.1.1 **Affinity Law** "for similar conditions of flow the capacity will vary directly with the ratio of speed and/or impeller diameter and the head with the square of this ratio at the point of best efficiency".

1.1.2 **Model Law "**two geometrically similar pumps working against the same head will have similar flow conditions if they run at speeds inversely proportional to their size, and in that case their capacity will vary with the square of their size".

1.2 **Vibration and noise** Here we introduce mechanical noise source and methods for reducing noise.

1.2.1 **Mechanical noise source** the two comely used mechanical noise sources are

described as: (a) Common mechanical sources that may produce noise include vibrating pump components or surfaces because of the pressure vibration that are generating in the liquid or air. Example: Impeller or seal rubs, Vibrating pipe walls, unbalanced rotors. (b) In centrifugal machines, improper installation of couplings often causes mechanical vibration at twice pump steep.

1.2.2 **Methods for reducing noise** the following are the comely used methods for reducing noise inside a mechanical operates. (a) Increase or decrease the pump speed to avoid system resonances of the mechanical system. (b) Decrease suction lift, increase air pressure. (c) Suction pipe should be straight.

According to Bernoulli [3] the differential pressure equation is given by

$$\frac{P_1}{\rho}+\frac{V_1^2}{2}+Z_1 g=\frac{P_2}{\rho}+\frac{V_2}{2}+Z_2 g \qquad (1)$$

$V_2 = 0$; $Z_1 = Z_2$.

The difference pressure equation is given by

$$(P_2-P_1)=\frac{V^2*\rho}{2} \qquad (2)$$

Where

P_1 =Initial pressure at the inlet of the impeller, in bar

P_2 = Final pressure at the outlet of the impeller, in bar

ρ = Density of air in kg/m^3

V =Velocity of air in m/s

It is well known [4, 5, 6] that three dimensional flow characteristic for an impeller of an axial turbo fan for improving the airflow rate and the static pressure. To consider an incompressible steady three-dimensional flow, the Reynolds (RANS) equations are used as

the governing equations, and the standard k-ε turbulence model is chosen. The pitch angles of 44°, 54°, 59°, and 64° are implemented for the numerical model. The numerical results show that airflow rates of each pitch angle are 1,175 CMH, 1,270 CMH, 1,340CMH, and 800 CMH, respectively. The difference of the static pressure at impeller inlet and outlet are 120 Pa, 214 Pa, 242 Pa, and 60Pa according to respective pitch angles. It means that the 59° of the impeller pitch angle is optimal to improve the airflow rate and the static pressure.

Also it is known that [7, 8] the turbo machinery flow is unsteady due to the relative motion between different components of the machine: for example the impeller blade passing in front of the stator vanes or in front of the tongue of the volute. Furthermore, in hydraulic machines the flow is fully turbulent and three-dimensional. Computing the entire real flow (unsteady and turbulent) through the whole pump requires a large computer memory and computational time even for the most performing computers [9]. Thus, a simplified simulation technique must be used in order to obtain useful results in a storage pump.

A finite element based method has been developed [10] for computing fluid-induced forces on an impeller in a volute casing. Potential flow theory is used assuming irrigational, in viscid and incompressible flow. Both excitation forces and motion dependent forces are calculated. The numerical results are compared with experimental results obtained at the California Institute of Technology. In two-dimensional and three-dimensional simulations the calculated pump characteristics near the design point are about 20% higher than the experimental curve. This is caused by viscous losses that are not taken into

account in our model. The magnitude of the excitation force is predicted well for optimum and high flow rates. At low flow rates the calculated force is too large which is probably related to inaccuracies in the calculated pressure.

2. COMPUTATIONAL FLUID DYNAMICS (CFD)

2.1 Methods and Governing Equations

CFD solvers are usually based on the finite volume method that includes the following steps: (a) Domain is discredited into a finite set of control volumes or cells. (b) General conservation or transport equation for mass, momentum, energy, etc., are discredited into algebraic equations which are shown in fig2. (c) All equations are solved to render flow field. (d) Governing differential equations become algebraic. (e) The collection of cells is called the grid or mesh. (f) System of equations is solved simultaneously to provide solutions.

CFD applies numerical methods called discretization to develop approximations of the governing equations of fluid mechanics and the fluid region to be studied. The set of approximating equations are solved numerically for the flow field variables at each node.

$$\frac{\partial}{\partial t}\int_v \rho\ \emptyset dv + \oint_A \rho \emptyset V\ .dA\ =\ \oint_A \Gamma\ \nabla\emptyset\ .dA + \int_V s_\emptyset\ dV$$

<Unsteady> + <Convention> =
<Diffusion> + <Generation>

Fig 2: General conversation

To keep the details simple, we illustrate the fundamental ideas underlying CFD by applying them to the following simple first order differential equation [11]:

$$\frac{du}{dx} + u_m = 0; 0 \le x \le 1; u(0) = 1 \quad (3)$$

It first considers the case where *m* = 1 when the equation is linear. This later considers the case where m = 2 when the equation is nonlinear. This derives a discrete representation of the above equation with *m* = 1 on the following grid:

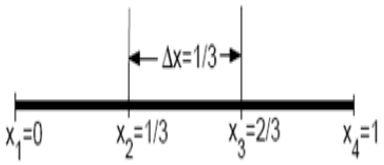

This grid has four equally-spaced grid points with Δx being the spacing between successive points. Since the governing equation is valid at any grid point, we have

$$\left[\frac{du}{dx}\right]_i + u_i = 0. \quad (4)$$

Here the subscript i represents the value at grid point x_i. In order to get an expression for $(du/dx)\ i$ in terms of u at the grid points, we expand u_{i-1} in a Taylor's series as

$$u_{i-1} = u_i - \Delta x \left[\frac{du}{dx}\right] + o(\Delta x^2). \quad (5)$$

A simple rearrangement of (5) gives

$$\left[\frac{du}{dx}\right]_i = \frac{u_i - u_{i-1}}{\Delta x} + o(\Delta x). \quad (6)$$

The error in $(du/dx)_i$, due to the neglected terms in the Taylor's series, is called the truncation error. Since the truncation error is $O(\Delta x)$, this discrete representation is termed first order accurate. Using (6) in (5) and excluding higher-order terms in the Taylor's series, we get the discrete equation as

$$\frac{u_i - u_{i-1}}{\Delta x} + u_i = 0 \quad (7)$$

This method of deriving the discrete equation using Taylor's series expansions is called the finite-difference method. However, most commercial CFD codes use the finite-volume or finite-element methods which are better suited for modeling flow past complex geometries. For example, the fluent code uses the finite-volume method whereas ansys (software) uses the finite-element method.

3. CFD Procedure and Analysis

Fluid flow analysis performed on the impeller, using ansys CFX. Numerical results fully characterized the flow field, providing detailed flow information such as flow speed, flow

angle, pressure, boundary layer development, losses. The flow field information from CFD simulation was then used to help elucidate the flow physics [12]. Impeller, blade geometry is shown in fig. 3 and fig. 4. Impeller design specification is shown in table 1.

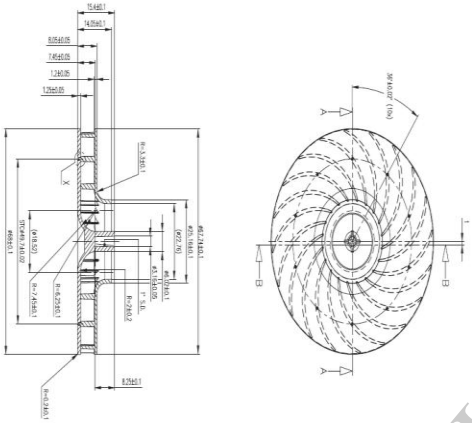

Fig.3. Impeller geometry front view and side view

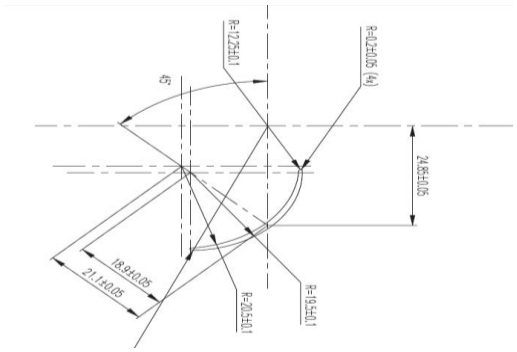

Fig.4. Blade geometry

S. No.	Parameter	Size
1.	Inlet diameter (D_i)	22.67 mm
2.	Outlet diameter(D_0)	67.74 mm
3.	Blade number	20
4.	Inlet angle (α)	38^o
5.	Outlet angle (β)	82^0
6.	Blade thickness (t)	2.5 mm
7.	Shaft diameter (D_s)	6 mm

Table1. Design specification of Impeller

3.1 Meshing

Turbo grid uses unstructured meshes in order to reduce the amount of time spent generating meshes, simplifying the geometry modeling and mesh generation process, model more complex geometries than can be handled with conventional, multi-block structured meshes, and let the mesh to be adapted to resolve the flow-field features. This flexibility allows picking mesh topologies that are best suited for particular application. The geometry is created by using Solid Works and the extruded geometry is meshed by Turbo Grid. Meshing of Single Blade and 20 blades Impeller is shown in fig. 6 and fig.7.Mesh

statistics and comparison between Classical model and new model is shown in tab.2 and tab3

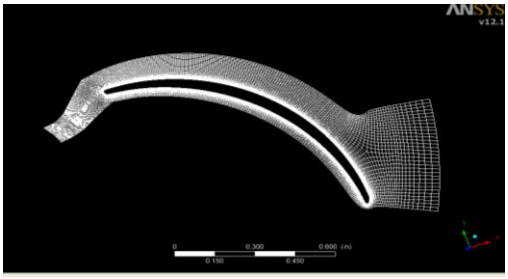

Fig.6. Meshing of Single Blade

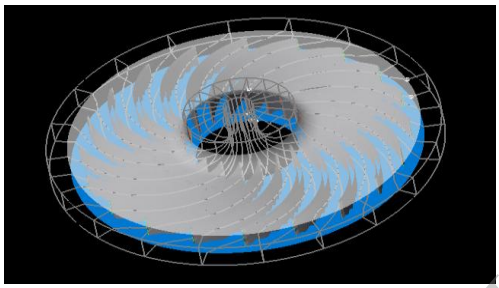

Fig.7. 20 blades Impeller

S. No.	Mesh measure	Value
1.	Minimum face angle	26.2748
2.	Maximum face angle	153.725
3.	Maximum element	382,072
4.	Minimum volume	1,74683e-012 [inches]
5.	Maximum edge	1970.8

Table.2. Mesh Statistics

S. No.	Parameter	Classical model	New model	Benefits of New model
1.	Inlet angle	55^0	38^0	Flow increment
2.	Outlet angle	75^0	82^0	Flow increment
3.	Number of blades	6	20	Flow increment
4.	Material	Steel	ABS (C_8H_8)	Cost reduction
5.	Outlet velocity	26.22 m/s	35.46 m/s	Outlet velocity increment

Table.3. Comparison between Classical model and new model

3.2 CFX Preprocessor

In the present work, the effect of inflow/outflow boundary conditions on the impeller is studied. Two types of inflow/outflow conditions are considered, static inflow with extrapolated outflow boundary condition 1(BC1), and dynamic inflow boundary condition 2 (BC2) that accounts for upstream influence in the subsonic flow. For the current problem air as ideal gas has been chosen these have the following properties. The values of fluid are shown in tab.4.

Molar mass	28.96 kg/ kmol
Density	1.024 kg/m³

Tab.4. Values of fluid

3.2.1 Wall Boundary Conditions

No-slip conditions were prescribed on the impeller blade surface surface. Zero Neumann boundary condition was imposed for pressure at the walls.

3.3 CFX Postprocessor

In this we can view the results such as contours, vectors and streamlines. In the results velocity contour, total pressure and pressure contours are shown.

4. Results and Discussion

Static pressure contours at 10000 rpm, 8000 rpm, 6000 rpm, 4000 rpm, and 2000 rpm at 70 % are shown in the following figures 8a, 8b, 8c, 8d and 8e:

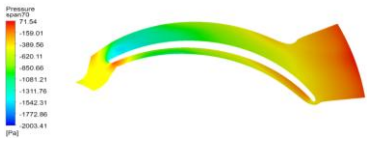

Fig.8a. 10000 rpm

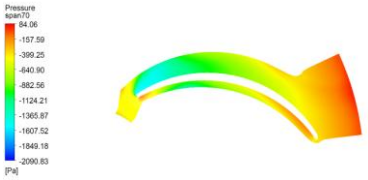

Fig.8b. 8000 rpm

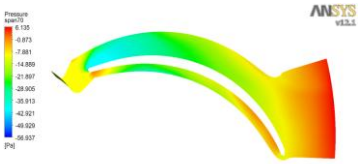

Fig.8c. 6000 rpm

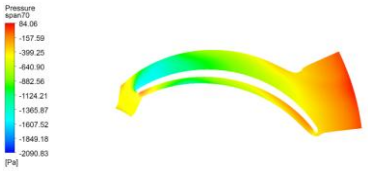

Fig.8d. 4000 rpm

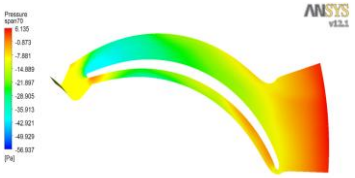

Fig.8e: 2000 rpm

As Sean in the figures the pressure distribution will vary as the speed of the impeller changes. From fig 8a the pressure at inlet is as compared to the pressure at outlet in 10000 rpm case but in the 2000 rpm case the pressure at inlet is

low and the pressure at outlet is high that means the exit velocity in 2000 rpm is low as compared to 10000 rpm.

Total Pressure contours at 10000 rpm, 8000 rpm, 6000 rpm, 4000 rpm, and 2000 rpm at 70 % are shown in the fooling figures 9a, 9b, 9c, 9d and 9e:

Fig.9a. 10000 rpm

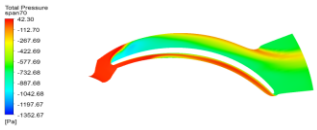

Fig.9b. 8000 rpm

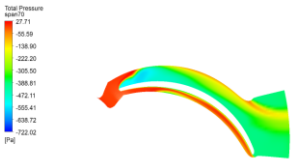

Fig.9c. 6000 rpm

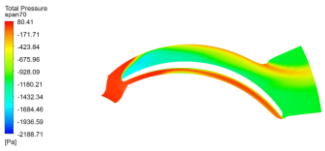

Fig.9d. 4000 rpm

Fig.9e. 2000 rpm

Profiles of span wise velocity component are shown in Figs for 10000 rpm, 8000 rpm, 6000 rpm, 4000 rpm and 2000 rpm respectively. The figures X axis represents axial chord and Y axis represents velocity in m/s. the figures represents flow variations in 10000 rpm , 8000 rpm , 6000 rpm , 4000 rpm and 2000 rpm at contours 20% , 50%, 70% span wise.

4.1 Mean span wise pressure profiles

Mean contours of span wise pressure component are shown in Figs for 10000 rpm , 8000 rpm, 6000 rpm, 4000 rpm and 2000 rpm respectively. The figures X axis represents axial chord and Y axis represents pressure in Pa. the figures represents flow variations in 10000 rpm , 8000 rpm , 6000 rpm , 4000 rpm and 2000 rpm at contours 20% , 50%, 70% span wise. Static pressure contours at 20%, 50% and 70% at 8000 rpm and10000 rpm is shown in fig.10a and fig.10b.

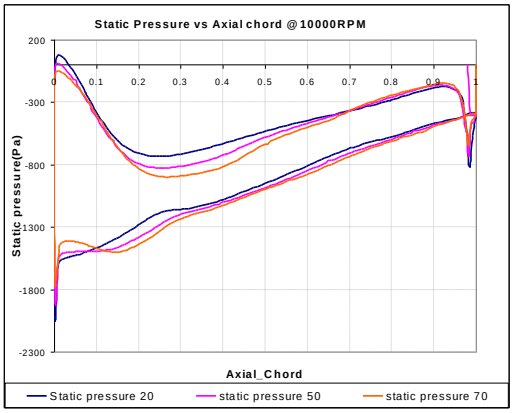

Fig.10a Static pressure contours at 20%, 50% and 70% at10000 rpm

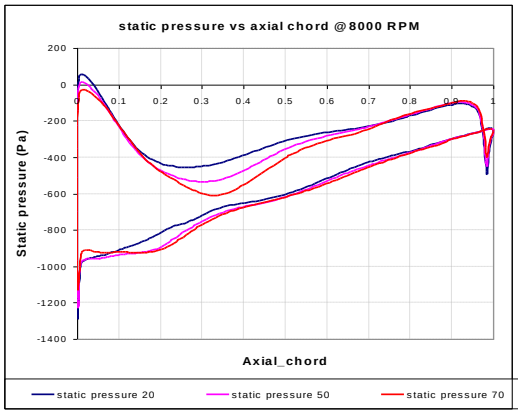

Fig.10b Static pressure contours at 20%, 50% and 70% at 8000 rpm.

4.2 Mean Span wise total pressure profiles

Mean contours of span wise total pressure component are shown in Figs for 10000 rpm , 8000 rpm, 6000 rpm, 4000 rpm and 2000 rpm respectively. The figures X axis represents axial chord and Y axis represents total pressure in Pa. the figures represents flow variations in 10000 rpm , 8000 rpm , 6000 rpm , 4000 rpm and 2000 rpm at contours 20% , 50%, 70% span wise at outlet. Total pressure profile 20%, 50% and 70% at 10000 rpm and head vs discharge is shown in fig.11 and fig. 12.

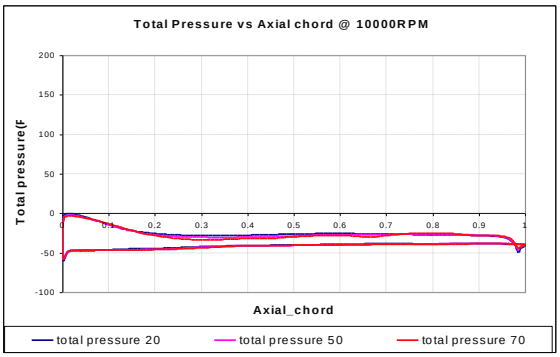

Fig.11. 20%, 50% and 70% at 10000 rpm

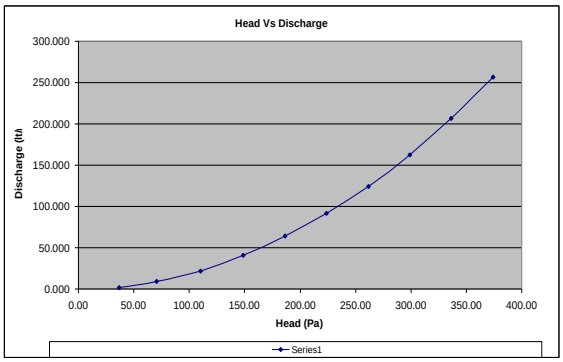

Fig.12: Head vs Discharge

The graph shows head vs discharge- axis represents head in Pa and Y-axis represents discharge in m^3 /s. The above graph shows there is no formation of surge and stall.

4.3 RPM vs Mass flow rate

The graph shows at different rpms (10000, 8000, 6000, 4000 and 2000) the behavior of fluid flow at outlet. If the rpm increases the flow at outlet will also increases. From the figure X-axis represents rpm and Y-axis represents mass flow rate in kg/s. Rpm vs Mass flow rate

(10000, 8000, 6000, 4000 and 2000 rpm) is shown in fig.13.

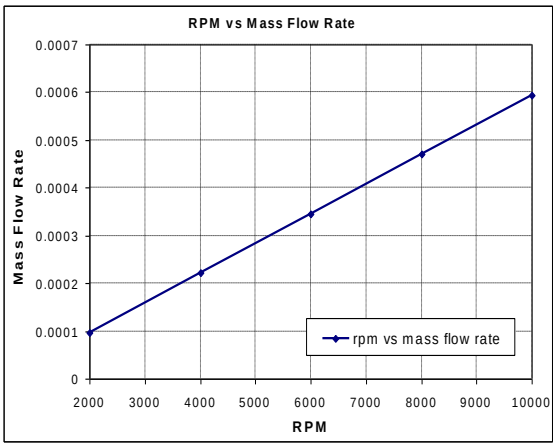

Fig.13. Rpm vs Mass flow rate (10000, 8000, 6000, 4000 and 2000 rpm)

5. Conclusions and Scope

Analysis was carried out for CFD cases for RPM of 10000, 8000, 6000, 4000 and 2000. It has been observed that all the cases are free from surge and stall. Velocity obtained from the CFD predictions of 35.46 m/s is achieved at outlet for the 10000 rpm case. There is no formation of wake in any of the cases. It has been observed that velocity of the fluid is directly proportional to impeller's RPM.Correlation has been derived between Head and Discharge. Correlation has been derived between RPM and Mass flow rate.

Future work should involve advancing the solution further in time for dynamic inflow or outflow boundary condition; and all the present simulations may be performed on a finer grid. Grid refinement may be done in order to obtain accurate results in both span wise as well as pitch wise direction.

6. Acknowledgements

My profound thanks are due to the referee for his valuable and constructive comments and to Dr. Koya Purnachandra Rao for his stimulating discussions.

7. Reference

[1] Labanoff Robert R. Ross, Centrifugal blower impeller design & application Gulf Publishing Company, Houston, TX, 1992, volume-2.

[2] T. E. Stirling: "Analysis of the design of two pumps using NEL methods" Centrifugal Pumps-Hydraulic Design-I Mech E Conference Publications 1982-11, C/183/82.

[3] Numerical Calculation of the flow in a centrifugal blower impeller using Cartesian grid procedure of 2nd WSEAS international Conference on applied and theoretical mechanics, Venice, Italy, November20-22,2006,According to john S. Anagnostopoulos.

[4] Young-Kyun Kim, Tae-Gu Lee, Jin-Huek Hur, Sung-Jae Moon, and Jae-Heon Lee World Academy of Science, Engineering and Technology 50 2009.

[5] International Journal of Rotating Machinery 2005:1, 45–522005 Hindawi Publishing Corporation Mechanical and Fluids Engineering Department, Southwest Research Institute, 6220 Culebra Road, an Antonio, TX 78238-5166, USA.

[6] MA Xi-jin, ZHANG Huachuan, ZHANG Kewei. Numerical Simulation and Experiment Analysis of Thirdly Circulating Feed-water Mixed-flow Pump in Nuclear Power Station. FLUID MACHINERY. Vol.37, No.09, 2009 6-9.

[7] Georgiana DUNCA1, Sebastian MUNTEAN 2, Eugen Constantin ISBĂŞOIU3, U.P.B. Sci. Bull., Series D, Vol. 72, Iss. 1, 2010.

[8] Miner S.M. 2001, 3-D viscous flow analysis of a mixed flow pump impeller, International Journal of Rotating Machinery, Vol. 7, No. l, pp. 53-63.

[9] Prepared for the33rd Joint Propulsion Conference and Exhibit cosponsored by AIAA**,** ASME, SAE, and ASEE Seattle, Washington, July 6–9, 1997.

[10] The 1997 ASME Fluids Engineering Division Summer Meeting FEDSM'97, June 22–26, 1997.

[11] Yun Chuan-yuan. Numerical Calculation of Turbulent Flow, Performance Experiment Mixed-flow Pump Impeller. Transactions of the Chinese Society for Agricultural Machinery. V01.39, No.3 2008. 52-55.

[12] JIA Rui-xuan, XU Hong. Optimal design of low specific speed mixed-flow pumps impeller. Journal of Drainage Irrigation Machinery Engineering. Vol. No.02, 2010, 98-102.